Dynamic control of propagating electromagnetic waves using tailored millimeter plasmas on microstrip structures

Sakai, O; Tachibana, K

Dynamic Control of Propagating Electromagnetic Waves Using Tailored Millimeter Plasmas on Microstrip Structures

Osamu Sakai, *Member, IEEE,* and Kunihide Tachibana, *Member, IEEE*

***Abstract*—Millimeter plasmas were tailored to play a role as dynamic devices of microwave components, that is, to control electromagnetic wave propagation dynamically on a microstrip line. The generation of millimeter plasmas with their relatively long discharge channel (∼3 mm) was in high-pressure (20–200 torr) Ne, and they were successfully arranged near and on the conductor of microstrip lines. When such a plasma was set perpendicularly to the conductor to form a T junction, a significant reduction of electromagnetic wave transmission along the metal conductor was observed. The reduction rate depended on the discharge current and the number of T junctions. These experimental results are compared with the case of 2 MHz launching for crude electron density measurements and the numerical results of propagating electric fields in a two-dimensional model.**

***Index Terms*—Electromagnetic propagation, glow discharges, microwave devices, numerical analysis.**

I. Introduction

MICROWAVE circuits developed so far have been composed of solid-state devices and are difficult to change their components in a time-varying manner. Here, our focus is on *plasma* devices for the dynamic control of microwaves and, in a broader sense, electromagnetic wave propagation. Interaction between electromagnetic waves and plasmas has been explored for several decades in various fields, such as ionosphere ionized layers [1], fusion plasmas [2], and plasma materials-processing reactors [3]. When electromagnetic waves are launched in or near nonmagnetized plasmas, they are transmitted, reflected, or absorbed according to the ratio of the electromagnetic wave frequency to the plasma frequency, which is a function of electron density. In other words, plasmas equivalently behave as conductors or dielectric materials for electromagnetic waves. These well-known facts are applicable to the development of electromagnetic-wave control devices composed of plasmas [4]–[6]. For instance, Borg *et al.* reviewed their experimental results on the application of very high frequency (VHF) excited plasmas to antennas [5]. As mentioned in previous reports, one can potentially obtain a dynamic (time-varying) electromagnetic wave controller made of plasmas. Recently, we reported time-varying electromagnetic wave attenuation through a sheet-like microplasma assembly [7].

Manuscript received April 22, 2005; revised July 30, 2005. This work was supported by a Grants-in-Aid for Scientific Research from the Japanese Ministry of Education, Culture, Sports, Science, and Technology.

The authors are with the Department of Electronic Science and Engineering, Kyoto University, Nishikyo-ku, Kyoto 615-8510, Japan (e-mail: osakai@kuee.kyoto-u.ac.jp).

Digital Object Identifier 10.1109/TPS.2005.863594

In this paper, we concentrate on plasma generation in a coplanar electrode configuration in an open space without discharge cells, which matches the widely used microstrip line technology in microwave circuits with a two-dimensional (2-D) conductor arrangement [8], [9]. The general frequency of electromagnetic waves propagating in the microstrip line $\omega/2\pi$ is set in a range from 1 to 10 GHz. If the frequency is set to 10 GHz, the wavelength is around 16 mm in the microstrip line, and so the required characteristic length of the plasmas to control electromagnetic waves is at least several millimeters, and the necessary electron density n_e for $\omega < \omega_{pe}$ is more than 10^{12} cm^{-3}, where ω_{pe} is the electron plasma frequency. One typical coplanar discharge is observed in a plasma display panel, where n_e is around 10^{13} cm^{-3} at its working gas (Ne in majority) pressure for 300–500 torr [10], [11], which fulfills the required condition of n_e. However, its discharge length is less than 1 mm, which is far from the required discharge length to control electromagnetic wave propagation. To overcome this problem, a three-electrode structure [12], [13] was adapted in our experiment to generate long-channel discharge with fairly high electron density. Another proposed scheme reported here is the tailored arrangement of multiplasmas on a microstrip line structure. Several reports showed the effects of multiplasmas in a one-dimensional periodical structure in which the dispersion relation of electromagnetic waves was significantly modified [6], [14], [15], although such a structure is not directly applicable to specific devices. For electron density measurements, 10-GHz wave transmission was investigated in a plasma-filled stripline structure [16], but its plasma structure was neither localized nor controlled. When combining the production of localized coplanar discharges with microstrip line technology, many other types of tailored arrangement can function to control electromagnetic wave propagation and contribute to develop such plasmas for specific devices.

In this paper, we would like to show our experimental results on the dynamic control of electromagnetic waves propagating in the microstrip line by generating elaborately arranged plasmas. First of all, plasma production in a relatively long (∼3 mm) discharge channel for 20–200 torr was successfully observed. Second, such plasmas were set near the conductor of the microstrip line to form a T junction, and electromagnetic wave transmission at 8–12 GHz was examined in relation to the discharge currents. T junction structure is just one typical microstrip line component, but it is a good example for evaluating the effects of a plasma that plays a crucial role in the determination of the boundary conditions of electromagnetic

wave propagation. These experimental results were compared with 2-MHz launching where a rough estimation of n_e was attempted, and a numerical calculation of a 2-D model reinforces those experimental results and clarifies the mechanisms of the observed electromagnetic wave attenuation. In Section II, the experimental setup is shown with descriptions of the pattern formation of the conductor and the electrodes. In Section III, the experimental results are presented in both terms of discharge identification and the demonstration of electromagnetic wave control, and in addition, 2-MHz launching is shown to derive electric conductivity and n_e in the discharge. In Section IV, the numerical analysis of wave equation in a 2-D model is described to explain the observed electromagnetic wave attenuation, which is followed by a conclusion in Section V.

II. Experimental Setup

A. Conductor and Electrode Arrangement on a Microstrip Line

A substrate of microstrip line was made from an ordinary glass epoxy copper clad laminate. Copper film 35 μm thick on the front side formed patterns of the conductor and the discharge electrodes for plasma generation. On the back side, the entire surface was covered with copper film at the ground potential level. The dielectric layer (glass base with epoxy resin, relative permittivity: 4.5) had a thickness of 1.6 mm.

The characteristic impedance of the microstrip line was set at 50 Ω by adjusting the conductor width to 3.0 mm [8]. The conductor and the discharge electrodes were formed in the following sequential process. First, a polyimide film (Kapton (R), DuPont de Nemours) was attached to the surface of the copper film, and a laser direct writing system (NEOARK, DDB-355-KTS) formed a positive pattern of conductor and electrodes by cutting the polyimide tape. After a copper film outside the pattern was removed by a wet etching process using $FeCl_3$ solvent, the polyimide tape was cut again by the laser direct writing system to distinguish the exposed areas of the copper film, including the electrode surface. Finally, the other area was covered by SiO_2 coating film.

B. Setup of Discharge Chamber and Microwave Circuit

The microstrip substrate was set in a stainless chamber pumped up to less than 0.1 torr before filled with discharge gas (Ne). Fig. 1 displays the schematic diagram of the microwave circuit in the experiment. Microwaves at frequencies ranging from 8 to 12 GHz, which were excited at the microwave source (Agilent Technology, 83 624B), were amplified by microwave amplifier [Kyoto-Micro-Densi, MRF-12G(3)] up to 3 W and delivered to the microstrip substrate. The characteristic impedance of all the lines where the electromagnetic waves propagate was kept at 50 Ω except high-pass filters (HPFs), which prevent discharge signals from disturbing the microwave amplifier and the output detector. The cutoff frequency of the high-pass filter was set at 75 MHz in cases of gigahertz wave injection. The transmission line was terminated by the characteristic impedance (50 Ω). The output signal was detected just before the terminator by a 6 dB directional coupler (MAC Technology, C3205-6) and a rectifier (Herotek, DZR185AA). The time evolution of the signals was displayed by digital oscilloscope (Iwatsu-Lecroy, LT344 500 MHz).

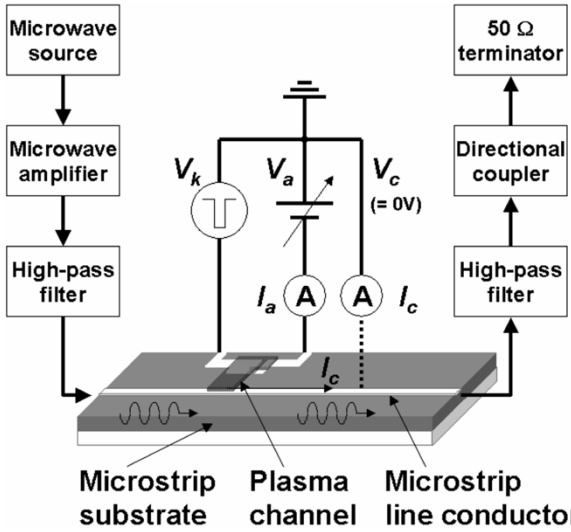

Fig. 1. Schematic view of plasma channel generation on microstrip line structure. Microwave circuit and plasma generation circuit are also shown. Real joint points of plasma generation circuit on the conductor (electrode) C are in HPFs.

A discharge electrode was driven in a negative square-shaped voltage pulse by a simple switching circuit using a p channel field-effect transistor (K1880, Renesas Technology) with 2-kΩ series resistance. The voltage pulse was applied on the cathode (K) electrode, and the electric potential at anode (A) electrode was controlled using a conventional direct-current power supply. Conductor (C) electrode, which was also in charge of the microstrip line conductor, was connected to the ground level through a 50-Ω resistor in HPFs.

III. Experimental Results

A. Discharge Features

Discharges were generated on the microstrip substrate in a three-electrode configuration. Fig. 2(a) shows one unit of an electrode pattern used in the experiment. The horizontal electrode gap between K and A was 200 μm, and that between K and C was set at 3 mm. When we varied gas pressure p from 20 to 200 torr, a long-channel discharge between K and C took place, although its outlook varied according to relative electrode potential and p. Fig. 2(b) shows the visible discharge emission patterns in various conditions. In general, strong emission was always observed on the K surface due to the formation of a cathode fall. When C was floating, only the discharge between K and A was observed. When both C and A were connected to the ground potential level, the main discharge took place between K and A with vague emission between K and C. When the potential of A electrode (V_a) was set at -40 V while the C electrode was at 0 V, a clear long-channel discharge took place between K and C. In low-pressure cases $(p = 30)$ torr, the width of the discharge channel was 3 mm, which equaled the electrode width with its transverse uniformity. In this way, a temporary T-junction-like structure appeared. As p increased to 180 torr, emission brightened but the discharge tended to narrow its width, and we could not retain its width of 3 mm for $p > 200$ torr. In the pressure region from 20 to 200 torr, striation was always observed along the discharge channel.

Fig. 3 shows the discharge ignition condition as a function of p. When A was set at ground potential, the discharge gap

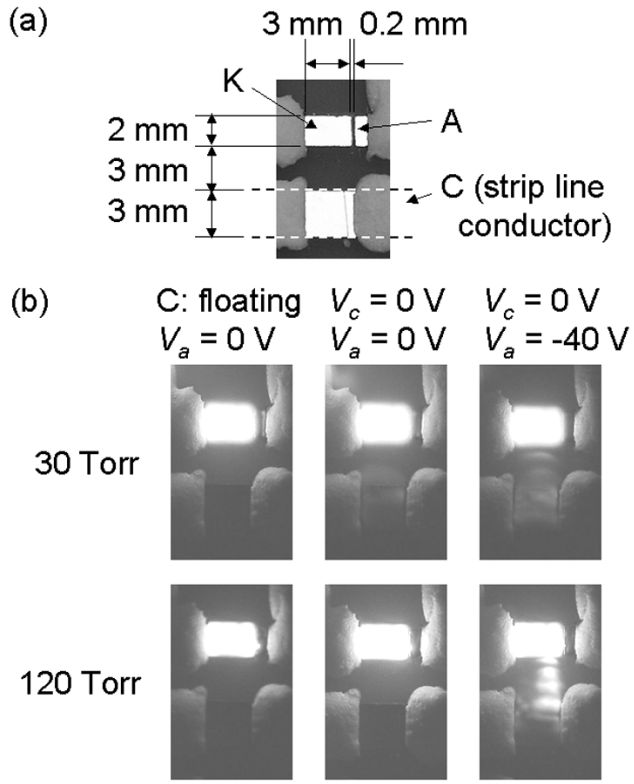

Fig. 2. (a) Top view of electrodes on microstrip line dielectric layer for electromagnetic wave transmission experiments. Inset values show specific size and distance about electrodes. (b) Visible emission patterns in cases of various electrode potential and gas (Ne) pressure.

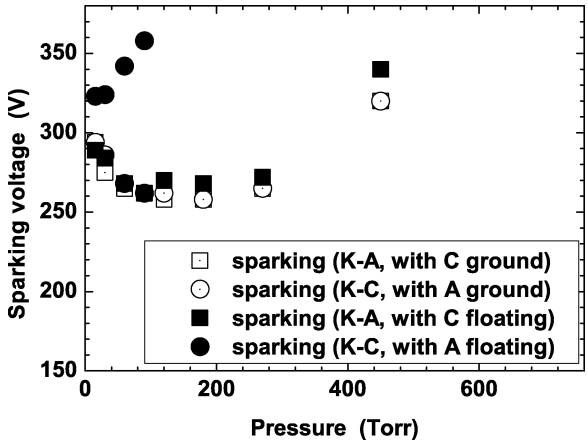

Fig. 3. Pressure dependence of sparking voltages in cases of various electrode potentials. $V_c = 0$ V and $V_a = 0$ V when not floating.

along the substrate surface was 200 μm, which is similar to the discharge gaps in ordinary plasma display panels [11]. The dependence on p was similar to the so-called Paschen characteristic and the minimum sparking voltage lay at $p = 150$–180 torr. When A was set in the floating condition, potential differences occurred between K and C. In this case, discharges took place only in the low-pressure region (less than 100 torr) and arc-like instability accompanied them. When both A and C were at ground potential, two channels were formed: one channel between K and A and another between K and C. Moreover, the ignition condition between K and C was similar to that between K

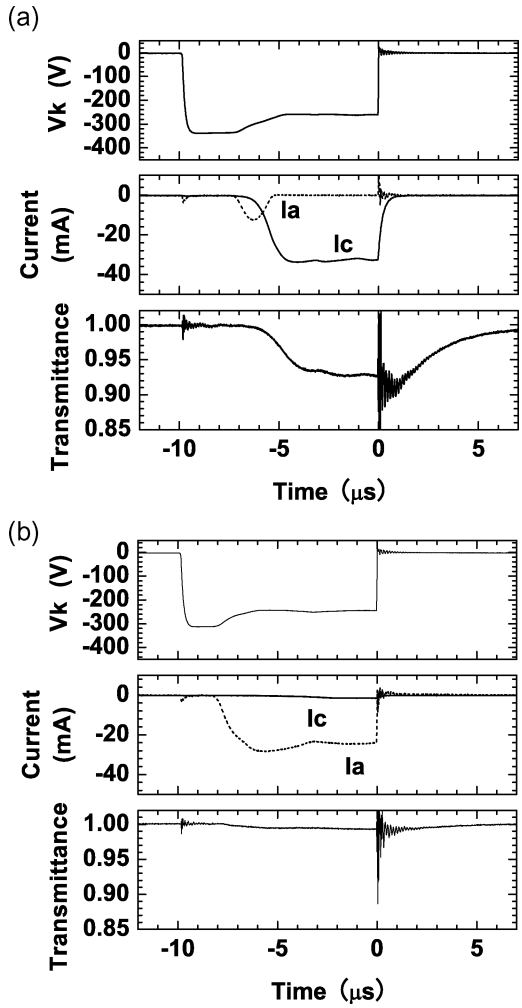

Fig. 4. (a) Time evolutions of V_k, I_c, I_a, and transmittance signals of electromagnetic waves at 11 GHz when $V_a = -50$ V and $p = 120$ torr. (b) Similar time evolutions to (a) when $V_a = -20$ V.

and A because of a triggering effect on longer channel coplanar discharge through a supply of charged particles from shorter channel coplanar discharge. Such a method was previously investigated in direct current microhollow discharges [17], [18] and in coaxial-hollow micro dielectric barrier discharges [19].

B. Electromagnetic Wave Transmission Through T Junctions Formed by One or Two Plasma Channels

As shown in Fig. 2(b), the relation between A electrode potential V_a and C electrode potential V_c determines the main discharge path. Fig. 4 demonstrates the time evolutions of the discharge signals and the corresponding electromagnetic wave propagation signal in two typical cases. Fig. 4(a) shows the temporal signals for $V_a = -50$ V and $V_c = 0$ V. The discharge current into A electrode I_a flowed at first, and discharge current into C electrode I_c followed. Simultaneously, the transmittance signal of 11.1-GHz electromagnetic wave decreased, and its attenuation tendency was very similar to the time evolution of I_c. On the other hand, Fig. 4(b) shows the case for $V_a = -20$ V and $V_c = 0$ V. I_a became saturated at a certain level, which never diminished, while the value of I_c was very small. As a result, transmittance was nearly constant with a very small drop that corresponds to I_a evolution.

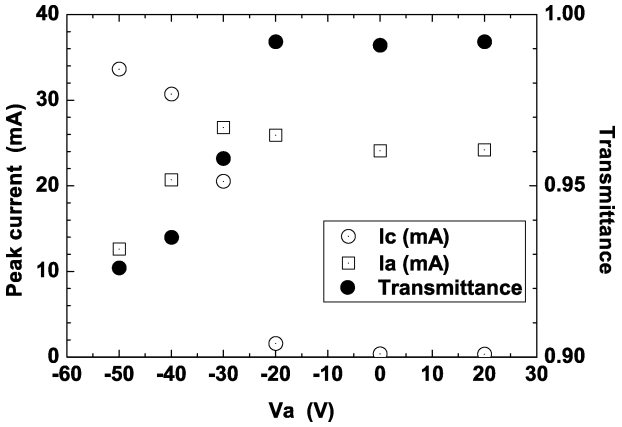

Fig. 5. V_a dependence of peak currents of I_c and I_a and electromagnetic wave transmittance at 11.1 GHz when gas pressure is 120 torr. V_k is set at $(V_a - 220)$ V during discharges.

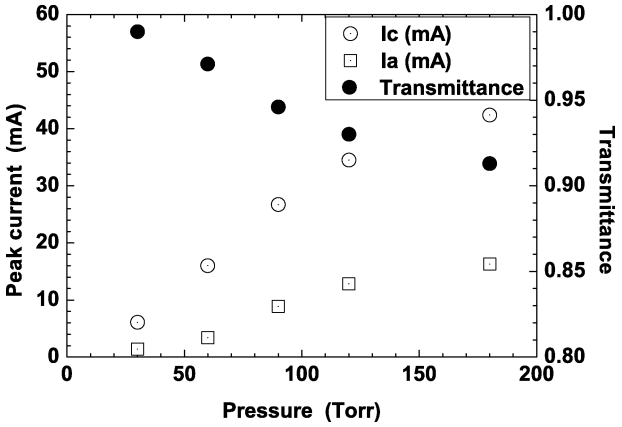

Fig. 6. Pressure dependence of peak currents of I_c and I_a and electromagnetic wave transmittance when $V_a = -50$ V. V_k is set at $-|(|V_s| + 20)|$V, where V_s indicates sparking voltage.

This attenuation tendency of the transmitted electromagnetic wave varied smoothly according to V_a shown in Fig. 5. Here, the voltage between K and A was kept constant, i.e., $V_k - V_a \sim -220$ V when I_c and/or I_a flowed. When V_a was negatively high, I_c flowed, and a reduction of transmittance was observed, which indicates a T-junction-like feature. With raising V_a to positive polarity, I_c gradually decreased and hardly flowed for V_a more than -20 V and simultaneously I_a increased to the saturation region. Attenuation was small, since it results from the existence of low-density plasma in the periphery region of the discharge between K and A. This result indicates that a larger voltage between K and C than between K and A is necessary to form a long-channel discharge between K and C.

To change I_c with a constant ratio of I_c to I_a, we varied p since the discharge currents increase with increasing p. The discharge currents are also controllable by changing V_k with constant p, but they cannot be lowered beneath a minimum value at the sparking voltage. Fig. 6 shows the p dependence of the discharge currents and the electromagnetic wave transmittance. The increase in the rate of wave attenuation was almost proportional to I_c. The maximum attenuation rate was about 9%, which was detected at 180 torr. From Figs. 5 and 6, we expect that electromagnetic wave transmittance in T-junction-like structure depends on I_c, which may be a function of n_e in a plasma channel.

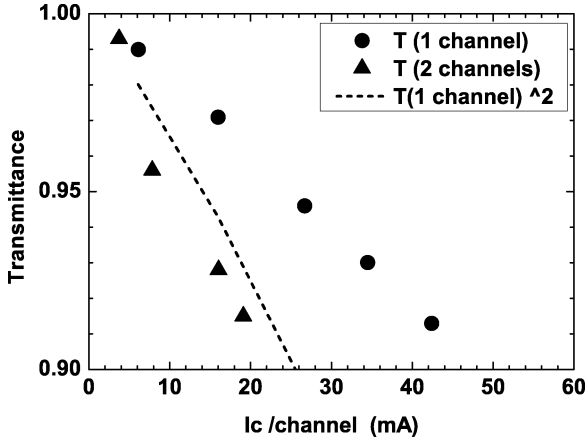

Fig. 7. Electromagnetic wave transmittance at 11.1 GHz normalized by I_c per one plasma channel when $V_a = -50$ V. V_k is set at $-|(|V_s| + 20)|V$. Dashed line indicates transmittance when attenuation of one plasma channel is simply doubled.

Fig. 7 shows the effects of multi-T junctions on electromagnetic wave attenuation. Two T junctions were formed on one microstrip line with a periodical length of 10 mm. With changing I_c by varying p, electromagnetic wave transmittance is plotted, normalized by I_c in one long-discharge channel. The dotted line indicates the doubled attenuation of the single T-junction data $(1-T^2$, where T is the transmittance in the case of single T junction). The experimental data of two T junctions show larger attenuation than $(1-T^2)$, partly because of a wave propagating effect similar to periodical T-junction structure used as a filter [8]. Fig. 8 shows electromagnetic wave frequency dependence of the attenuation normalized by I_c in one long-discharge channel. The tendency is complicated for two reasons: the straightway transmission of an ordinary T junction composed of a metal conductor increases from 52% to 62% as frequency increases from 7 to 10 GHz [20], and the fraction of electromagnetic wave energy carried in the plasma-channel area in cross section increases from 23% to 29% from a numerical analysis similar to that described in Section IV (not shown here). Unknown mutual inductance and capacitance and their coupling with plasma channels might affect this frequency dependence, too. A more important feature suggested in Fig. 8 is that, after doubling the T junctions in a similar case to Fig. 7, the attenuation ratio increased at 8 GHz. The periodical length of 10 mm fulfills the condition of half wavelengths of 8-GHz electromagnetic waves propagating in our microstrip substrate [8]. That is, this result may be further evidence that the observed attenuation arises from the modification of electromagnetic wave propagation affected by periodical structure.

C. *Transmission of 2-MHz Waves Through Plasma Channels*

So far we have investigated the effects of a dynamic T-junction-like structure on electromagnetic wave transmission. Further experiments were performed to reveal other aspects of these facts and accounts of observed electromagnetic wave attenuation.

If the plasma channels behave only as short-circuited stubs and attenuate the electromagnetic waves, low frequency waves would also decay through the T-junction structure. However, when we performed 2-MHz launching instead of microwaves, no attenuation (or less attenuation than the detection limit) was observed, indicating that a certain length in comparison with the

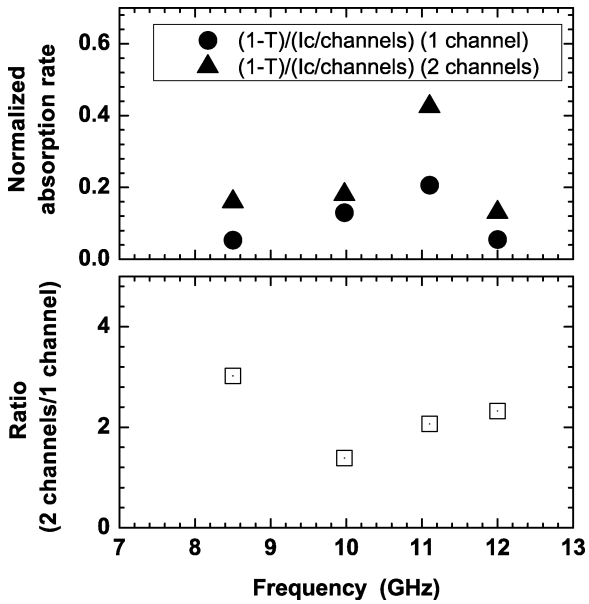

Fig. 8. Normalized absorption rate, defined as absorption rate divided by I_c per one plasma channel, and ratio of normalized absorption rate between one-and two-channel cases, as a function of electromagnetic wave frequency when $V_a = -50$ V. V_k is set at $-|(|V_s| + 20)|$V.

wavelength is required for plasma channels to control electromagnetic wave transmission.

2-MHz launching was also investigated to estimate the conductivity of plasma channels, assuming that the conductor and the plasma channels are equivalent to lumped-constant circuit elements at this frequency. To investigate the conductivity of the plasma channels, 2-MHz waves were transmitted through microstrip line gap structure filled with plasma channels, as shown in Fig. 9(a). Fig. 9(b) displays the time evolution of the discharge signals and the detected transmitted wave. The 2-MHz wave was launched at one end of the microstrip gap (C1) and propagated through the plasma channels, to reach the other end of the microstrip gap (C2). The detected wave amplitude, which was measured as a voltage drop across 100 Ω, was approximately 1/200 of the input wave amplitude at 120 torr. The detected signals were completely in phase with the input wave, and it is assumed that the plasma channels, which were replaced by $2R$, are in series to the external resistance (100 Ω, r). This assumption will be discussed further in Section IV. In this case, the equivalent resistance of the two plasma channels $2R$ is estimated to be around 20 kΩ. Fig. 10 displays the conductivity derived from relation $R = (1/\sigma)(l/S)$, where σ is the conductivity of the plasma channel, l is the plasma channel length, and S is a cross section of the plasma channel. The plasma channel was 3 mm wide. But its thickness was not clear and here we assume that it ranged from 0.2 to 0.5 mm, which corresponded to the thickness of the visible emission layer observed in the side views of the long-channel discharges. When the applied frequency is much less than the collision frequency, σ can be expressed using the following equation [21]:

$$\sigma = \frac{e^2 n_e}{m_e \nu_{\rm m}} \tag{1}$$

where e is the electron charge, m_e is the electron mass, and $\nu_{\rm m}$ is the electron momentum transfer frequency with $1.2 \times 10^9 (\mathrm{s}^{-1}\ \mathrm{torr}^{-1}) \times p(\mathrm{torr})$ in the case of Ne [21]. Calculating

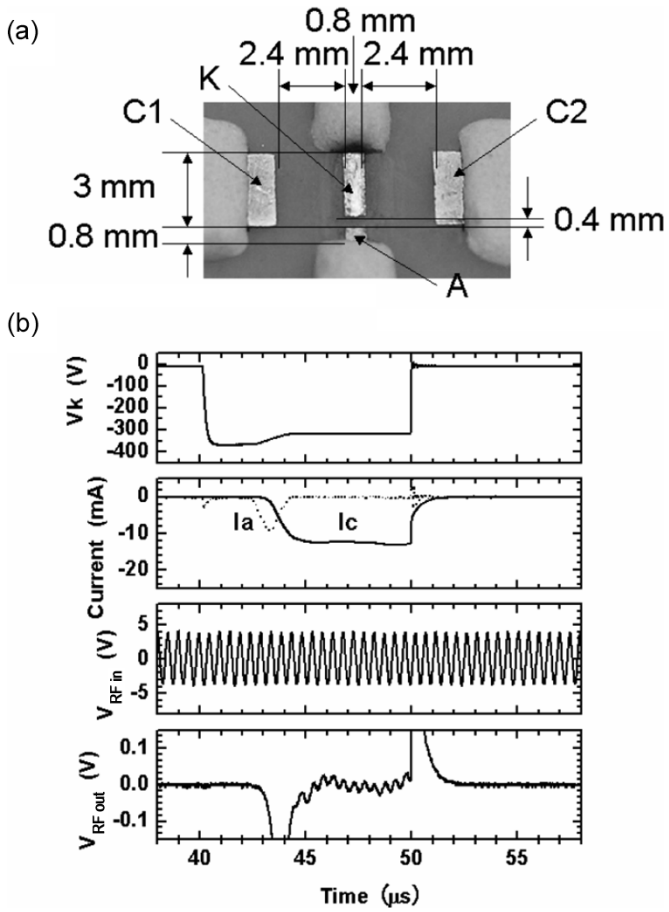

Fig. 9. (a) Top view of electrodes on microstrip line dielectric layer for conductivity measurements. Inset values show specific size and distance about electrodes. (b) Time evolutions of signals for conductivity measurements. $V_{\rm RFin}$ is 2 MHz wave amplitude before entering HPF on the side of C1, and $V_{\rm RFout}$ is the output signal on the side of C2 through HPF.

n_e using (1) on the assumption of its slab profile is also shown in Fig. 10. The tendency of n_e is very similar to I_c in Fig. 6, and so I_c as a function of p can be used as an alternative of relative n_e value. In Section IV, these derived n_e values will be compared to the numerical analysis.

IV. Discussion

Conductivity measurements using 2-MHz launching led to the estimation of averaged n_e, and here we mention the validity of the assumption that a 2-MHz equivalent circuit consists of R and $r(= 100\ \Omega)$ that are in a series. A more precise description is that the two anode sheaths on C1 and C2 play roles of capacitance (C_a), and the cathode fall region is equivalent to another capacitance (C_k) that is connected to the series resistance (2 kΩ, r_p) of the pulse voltage generator. Total impedance Z at the 2-MHz launching point is

$$Z = \frac{1}{j\omega C_a} + R + \left(\left(\frac{1}{j\omega C_a} + R + r \right)^{-1} + \left(\frac{1}{j\omega C_k} + r_p \right)^{-1} \right)^{-1}. \tag{2}$$

First of all, the experimental observation of no phase differences between the input and the output signals indicates that C_a is so large that the term of $(1/(j\omega C_a))$ is negligible. r_p

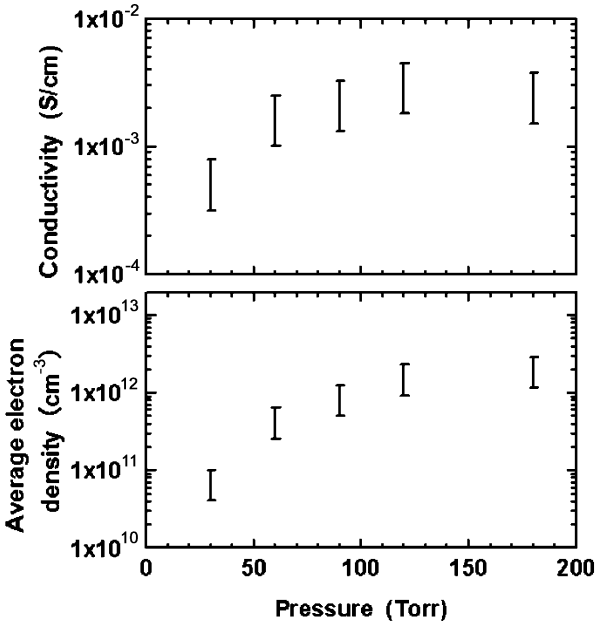

Fig. 10. Conductivity and n_e as a function of gas pressure. Conductivity is derived from the ratio of $V_{\mathrm{RF\ in}}$ and $V_{\mathrm{RF\ out}}$, and n_e is calculated from (1) using conductivity values. Error bars indicate the assumed plasma thickness ranging from 0.2 to 0.5 mm.

is at least several times smaller than R, and so R would become smaller than cases where r_p is ignored. As a result, n_e shows larger values if r_p is considered. When capacitance C_k is quite large and the term of $(1/(j\omega C_k))$ is ignored, estimation of $2R$ modified by (2) leads to 8 kΩ at 120 torr, which corresponds to $n_e = 1 \times 10^{13}$ cm^{-3}. Unfortunately, 2-MHz signal cannot be detected at K and A due to low signal-to-noise ratio, and no more experimental evidence can be used. Another factor that affects the derivation of n_e is its distribution along the discharge path. In general, n_e is not uniform in a glow discharge, and a lower density region would be less conductive. The influence of a low-conductive region is quite complicated. That is, n_e evaluation from low frequency wave transmission includes some errors, but its rough estimation may be valid, leading to $n_e = 10^{12} - 10^{13}$ cm^{-3}.

To reinforce the n_e estimation shown above, we numerically analyzed the 2-D cross-sectional distribution of electromagnetic waves. When external current density is assumed to be present, we solve the wave equation as

$$\nabla \times \nabla \times \boldsymbol{E} - \omega^2 \mu \varepsilon \boldsymbol{E} = j\omega\mu \boldsymbol{J}_{\mathrm{ext}} \tag{3}$$

using the finite difference method, where

$$\varepsilon = 1 - \left(\frac{\omega_{pe}}{\omega}\right)^2 \frac{1}{1 - j\left(\frac{\nu_{\mathrm{m}}}{\omega}\right)} \tag{4}$$

is the complex dielectric coefficient, μ is the permeability of free space, and $\boldsymbol{J}_{\mathbf{ext}}$ is the external current density. In the microstrip line, electromagnetic waves propagate in the quasi-TEM mode [8], and so it can be assumed that their fields are present only in the plane perpendicular to the wavenumber vector along the conductor line. Using this assumption, electric field $\boldsymbol{E}$ is divided into two components in the cross-sectional plane, i.e., E_x, which is the component along the electrode substrate, and E_y, which is the component perpendicular to the substrate. They are calculated as complex values to investigate relative phase to $\boldsymbol{J}_{\mathbf{ext}}$ that only has a real part. $\boldsymbol{E}$ is derived in the cross section including the long-channel discharge of the T-junction like structure shown in Fig. 11(a). $\boldsymbol{J}_{\mathbf{ext}}$ as an electromagnetic wave source at 11 GHz is assumed to flow at the midpoint of the conductor plane between the conductor and the grounded electrode. A uniform plasma 500 μm thick is set to bridge the conductor and the K electrode that is connected to the grounded level through r_p, and 100-μm-thick vacuum layers are arranged to simulate sheaths on the metal surfaces. On all the boundaries, the normal component of $\boldsymbol{E}$ is zero and the normal gradient of the tangential component of $\boldsymbol{E}$ is zero, which means that the boundary lines are on the symmetric axis of the periodical configuration. The conductor in Fig. 11(a) represents half of itself in the experimental structure.

Fig. 11(b), (c), and (d) shows $|\boldsymbol{E}|$ profiles for $n_e = 3 \times 10^{10}$, 3×10^{12}, and 3×10^{14} cm^{-3}, respectively. Each graph consists of profiles of the imaginary (E_i) and the real (E_r) part of $\mathbf{E}$. The condition of $\omega = \omega_{pe}$ at $\omega/2\pi = 11$ GHz corresponds to $n_e = 1.5 \times 10^{12}$ cm^{-3}. In low-density cases where $\omega \gg \omega_{pe}$ [Fig. 11(b)], only E_i is present, and no influence in the plasma region can be seen. On the other hand, in the case of $\omega \sim \omega_{pe}$ [Fig. 11(c)], E_i becomes weaker and E_r emerges in the plasma region, especially for $x < 1.5$ mm. E_r is in phase with $\boldsymbol{J}_{\mathbf{ext}}$, and so power dissipation via Joule heating occurs in accordance with E_r due to electron momentum collision. If gas pressure is set very low (e.g., <1 torr) and momentum collisions are rare, E_r will become very small and no power dissipation will take place even for $\omega \sim \omega_{pe}$. When n_e is raised to 3×10^{14} cm^{-3}, which is shown in Fig. 11(d) and corresponds to the case with $\omega \ll \omega_{pe}$, the plasma region behaves as a perfect conductor and almost no electric field is present inside it.

The density dependence of $|\boldsymbol{E}|$ distribution in the plasma region is displayed in Fig. 12, where the results of integrated E_i^2 and E_r^2 in the plasma area are shown. These values reflect the relative electric power carried or stored in space, although the absolute values cannot be compared since the stored electric energy density is $(\omega\varepsilon/2)E_i^2$, whereas the Joule heating term is expressed as $(\sigma/2)E_r^2$. As n_e is increased, the reduction of E_i^2 and the emergence of E_r^2 are observed near the condition of $\omega = \omega_{pe}$. Further increase of n_e leads to decreases of both E_i^2 and E_r^2. The experimental condition of n_e should correspond to $\omega \sim \omega_{pe}$ or $\omega < \omega_{pe}$, since the changes of E_i^2 and E_r^2 are in this region, which leads to the conclusion that n_e in the long-channel discharge was more than 10^{12} cm^{-3}. This was consistent with the experimentally estimated n_e by (1) shown in Fig. 10. One might consider that the observed electromagnetic wave attenuation is simply due to power dissipation if $\omega \sim \omega_{pe}$, but such is not the case. If impedance of space η is considered, electromagnetic wave reflection coefficient Γ is expressed as $(\eta - \eta_0)/(\eta + \eta_0)$, where η_0 is the impedance of the free space, and in a general conductor, $\eta = (1 + j)(\omega\mu/(2\sigma))$. That is, the transition from lossless to conductive medium originating from σ will cause electromagnetic wave propagation changes. Figs. 7 and 8 show phenomena that cannot be explained by the simple power dissipation model; there must be experimental evidence of the effective modification of electromagnetic wave propagation by the existence of long-plasma channels.

Recently, Iza *et al.* [22] and Kim *et al.* [23] showed that microplasmas can be ignited and/or sustained with less than 1 W

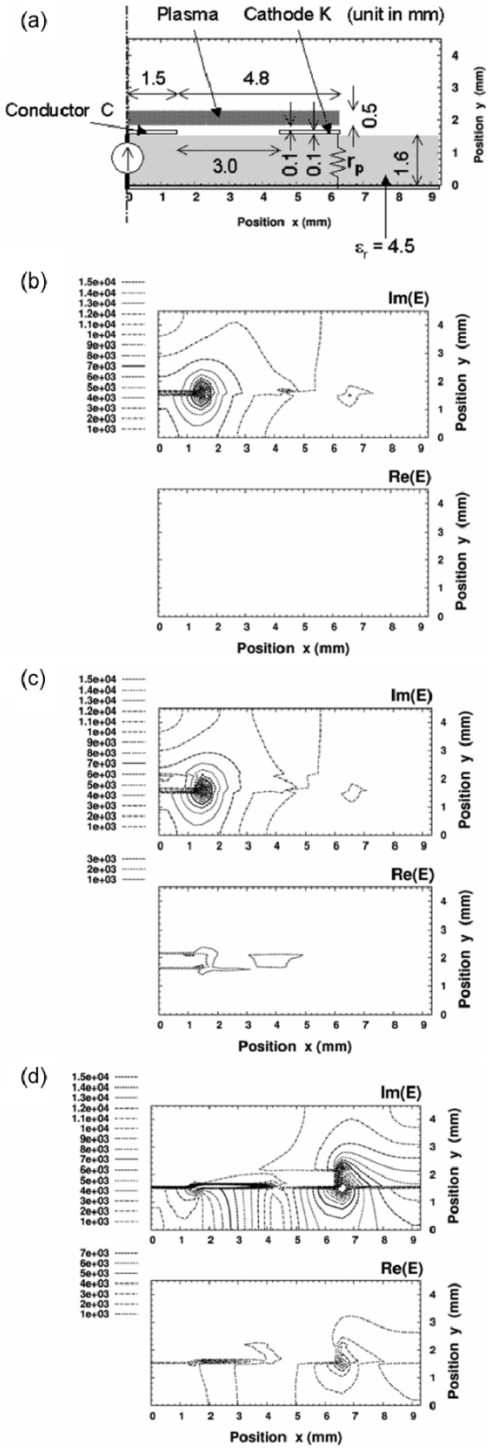

Fig. 11. (a) 2-D structure used in numerical analysis. External current source is set at position $x = 0$ mm for position $y = 0$–1.6 mm, and K is connected to the ground level through $r_p = 2\,\mathrm{k}\Omega$ at $x = 6.3$ mm. Grounded electrode at $y = 0$ mm, conductor C and electrode K at $y = 1.6$ mm are assumed to be perfect conductors. (b) Imaginary and real parts of electric field $\boldsymbol{E}$ of electromagnetic waves numerically calculated using (3) and (4) on assumption of structure in (a). n_e is set at 3×10^{10} cm^{-3} in the hatched region, and gas (Ne) pressure is assumed to be 120 torr. (c) Numerical results of $\boldsymbol{E}$ on assumption that $n_e = 3 \times 10^{12}$ cm^{-3}. (d) Numerical results of $\boldsymbol{E}$ on assumption that $n_e = 3 \times 10^{14}$ cm^{-3}.

of microwaves at 2.45 GHz or less. In our experiments transmitted power through a microstrip line was 1–2 W, and microwave dissipated power in a dynamic T junction was at most 0.1–0.2 W, which would not affect discharge property so much since a long-channel plasma was produced by the pulsed power

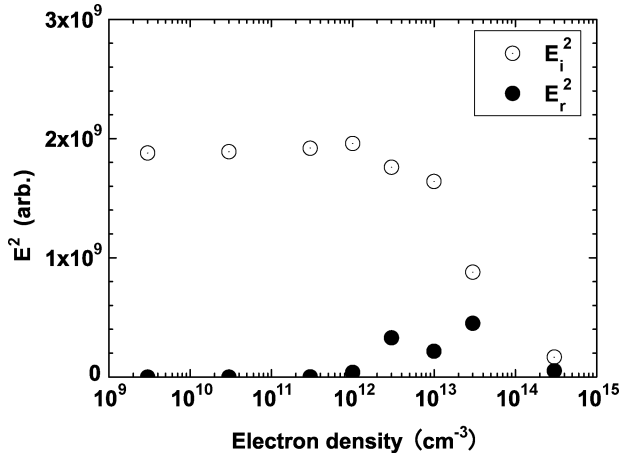

Fig. 12. Integration of imaginary and real parts of $|\boldsymbol{E}|^2$ in plasma channel region as a function of n_e, calculated using (3) and (4) on assumption of the structure in Fig. 11(a).

with about 10 W. If the dissipated power increases up to around 1 W for high-power microwave control, it might reduce slightly the threshold $(V_a - V_c)$ values for switching a long-channel plasma. However, the above-mentioned microplasmas sustained by microwaves were generated at electrode gaps less than 1 mm, whereas our long-channel plasma was 3 mm long and its discharge controllability will be maintained without crucial influences, even if microwave power is close to 100 W [24].

As mentioned above, the T-junction-like structure formed by a plasma channel has been discussed as an attenuator. However, a usual T junction plays the role of power divider. When one uses the T-junction-like structure shown here as a power divider, another conductor is necessary on the other side of K. In that case, however, the structure of a microstrip line gap will also be formed between the two conductors if the plasma is turned off, which complicates the plasma effects for discussion. Another point we should mention is the comparisons with the characteristic of the usual T junction composed of metal layers. The usual T junction shows 2-dB attenuation [20], or 37% attenuation from the input power at 10 GHz. In our T-junction-like structure, attenuation was at most 10%, which remained in a smaller level, partly because n_e was insufficient in comparison with a perfect conductor. Increase of n_e is possible when we reduce the pulsewidth of V_k, when V_k is increased with smaller r_p within the range without glow-to-arc transition, and/or when another gas species for more efficient plasma production is applied. For instance, when we made a dynamic T-junction-like structure by Ar gas discharge instead of Ne, attenuation about 2.5 times larger than the Ne case was observed at $p < 40$ torr (not shown here), mainly due to higher n_e in Ar. However, for more than 40 torr, the long-channel discharge could not be 3 mm wide and became unstable, and consequently replacement by Ar did not lead to stronger control of transmitted microwave power. Further optimization of gas composition might result in larger attenuation with discharge stability. Another way to enhance attenuation is to optimize energy flow path of transmitted waves. Recently, we observed large attenuation more than 25% by a dynamic T junction formed at right-angle bend, which will be reported elsewhere [25].

For specific applications, this dynamic T junction will develop into a high-speed microwave modulator with up to

1-MHz modulation frequency by a sinusoidal voltage signal for $(V_a - V_c)$. Furthermore, if 2-D plasma arrangements are modified from T junctions to other functional patterns, it will work as other devices, such as tunable impedance matchers and temporary filters.

Finally, note the potential of this scheme for applications to higher frequency waves. For instance, if the working gas pressure is raised to the atmospheric pressure, a plasma channel with $n_e > 10^{13}$ cm^{-3} and $l \sim 1$ mm will be created, which will be suitable to control the so-called Q band (33–50 GHz) millimeter waves: the concept itself is not limited within a certain frequency range, if the technology of gas containers can support the working gas pressure more than the atmospheric pressure.

V. Conclusion

We demonstrated the effects of plasmas on electromagnetic wave propagation on a microstrip line. Using a three-electrode configuration, long plasma channels in comparison to conventional coplanar glow discharges were successfully produced in Ne for 20–200 torr. The propagating electromagnetic wave was attenuated when the long plasma channels gave rise to T-junction structures. The attenuation rate showed a monotonous function of the strength of the plasma channels or the discharge current along them, which was directly related to electron density in the plasma channels. 2-D numerical analysis of the propagating electric field suggested that these experimental observations result from the change of media for electromagnetic waves from lossless space to good conductor according to ratio ω_{pe}/ω.

References

[1] V. L. Ginzburg, *The Propagation of Electromagnetic Waves in Plasmas*. Oxford, U.K.: Pergamon, 1964.
[2] T. H. Stix, *The Theory of Plasma Waves*. New York: McGraw-Hill, 1962.
[3] M. A. Lieberman and A. J. Lichtenberg, *Principles of Plasma Discharges and Materials Processing*. New York: Wiley, 1994.
[4] R. J. Vidmar, "On the use of atmospheric pressure plasmas as electromagnetic reflectors and absorbers," *IEEE Trans. Plasma Sci.*, vol. 18, no. 4, pp. 733–741, Aug. 2000.
[5] G. G. Borg, J. H. Harris, N. M. Martin, D. Thorncraft, R. Milliken, D. G. Miljak, B. Kwan, T. Ng, and J. Kircher, "Plasmas as antennas: theory, experiment and applications," *Phys. Plasmas*, vol. 7, pp. 2202–2198, May 2000.
[6] J. Faith, S. P. Kuo, and J. Huang, "Frequency downshifting and trapping of an electromagnetic wave by a rapidly created spatially periodic plasma," *Phys. Rev. E, Stat. Phys. Plasmas Fluids Relat.*, vol. 55, pp. 1843–1851, Feb. 1997.
[7] K. Tachibana, Y. Kishimoto, S. Kawai, T. Sakaguchi, and O. Sakai, "Diagnostics of microdischarge-integrated plasma sources for display and material processing," *Plasma Phys. Contr. Fusion*, vol. 47, pp. A167–A177, Apr. 2005.
[8] D. M. Pozar, *Microwave Engineering*. Reading, U.K.: Addison-Wesley, 1990.
[9] B. C. Wadell, *Transmission Line Design Handbook*. Norwood, MA: Artech House, 1991.
[10] Y. Noguchi, A. Matsuoka, K. Uchino, and K. Muraoka, "Direct measurement of electron density and temperature distributions in a micro-discharge plasma for a plasma display panel," *J. Appl. Phys.*, vol. 91, pp. 613–616, Jan. 2002.
[11] J. P. Bouef, "Plasma display panels: Physics, recent developments and key issues," *J. Phys. D, Appl. Phys.*, vol. 36, pp. R53–R79, Feb. 2003.
[12] O. Sakai, S. Hashimoto, and A. Hatano, "Switching and regulation of a pulsed discharge channel in a coplanar plasma tetrode," *Appl. Phys. Lett.*, vol. 82, pp. 2392–2394, Apr. 2003.
[13] O. Sakai, S. Hashimoto, and A. Hatano, "Flat triode structure with a pulsed coplanar discharge channel representing similar features to a field-effect transistor," *Appl. Phys. Lett.*, vol. 82, pp. 2781–2783, Apr. 2003.
[14] D. K. Kalluri, *Electromagnetics of Complex Media*. Boca Raton, FL: CRC, 1998.
[15] H. Hojo and A. Mase, "Dispersion relation of electromagnetic waves in one-dimensional plasma photonic crystals," *J. Plasma Fusion Res.*, vol. 80, pp. 89–90, Feb. 2004.
[16] L. F. Weber, "Measurement of a plasma in the AC plasma display panel using RF capacitance and microwave technique," *IEEE Trans. Electron Devices*, vol. ED-24, pp. 859–864, Jul. 1977.
[17] R. H. Stark and K. H. Schoenbach, "Direct current high-pressure discharges," *J. Appl. Phys.*, vol. 85, Feb. 1999.
[18] H. I. Park, T. I. Lee, K. W. Park, and H. K. Baik, "Formation and large-volume, high-pressure plasmas in microhollow cathode discharges," *Appl. Phys. Lett.*, vol. 82, pp. 3191–3193, May 2003.
[19] O. Sakai, Y. Kishimoto, and K. Tachibana, "Integrated coaxial-hollow micro dielectric-barrier-discharges for a large-area plasma source operating at around atmospheric pressure," *J. Phys. D, Appl. Phys.*, vol. 38, pp. 431–441, Jan. 2005.
[20] E. Mori, *Introduction Course of Microwave Technique* (in Japanese). Tokyo, Japan: CQ Publishing, 2003.
[21] Y. P. Raizer, *Gas Discharge Physics*. Berlin, Germany: Springer, 1987.
[22] F. Iza and J. A. Hopwood, "Low-power microwave plasma source based on a microstrip split-ring resonator," *IEEE Trans. Plasma Sci.*, vol. 31, no. 4, pp. 782–787, Aug. 2003.
[23] J. Kim and K. Terashima, "2.45 GHz microwave-excited atmospheric pressure air microplasmas based on microstrip technology," *Appl. Phys. Lett.*, vol. 86, pp. 191 504-1–191 504-3, May 2005.
[24] A. Kono, T. Sugiyama, T. Goto, H. Furuhashi, and Y. Uchida, "Production of CW high-density nonequilibrium plasma in the atmosphere using microgap discharge excited by microwaves," *Jpn. J. Appl. Phys.*, vol. 40, pp. L238–L241, Mar. 2001.
[25] O. Sakai, T. Sakaguchi, Y. Ito, and K. Tachibana, "Interaction and control of mm-waves with microplasma arrays," *Plasma Phys. Contr. Fusion*, vol. 47, pp. B617–B627, Nov. 2005.

Osamu Sakai (M'05) received the B.S., M.S., and Ph.D. degrees from Kyoto University, Kyoto, Japan, in 1990, 1992, and 1996, respectively. His major field of study for the Ph.D. degree was plasma heating and confinement using electromagnetic waves in mirror plasmas.

He was a Research Engineer of the Sharp Corporation, Nara, Japan, and is currently a Research Associate with the Department of Electronic Science and Engineering, Kyoto University. His current research interests include microplasmas and their application to electromagnetic wave controllers.

Dr. Sakai is a member of The Japan Society of Applied Physics and The Japan Society of Plasma Science and Nuclear Fusion Research.

Kunihide Tachibana (M'02) received the B.S., M.S., and Ph.D. degrees from Kyoto University, Kyoto, Japan, in 1968, 1970, and 1973, respectively.

He joined the Department of Electronics, Kyoto Institute of Technology, in 1974 and became a Full Professor in 1988. He moved to the Department of Electronic Science and Engineering, Kyoto University, in 1995 as a Full Professor. His research subjects include plasma diagnostics with lasers and other spectroscopic techniques in various kinds of plasmas for material processing, light sources, and display devices. His current research interest is shifting toward microplasmas and atmospheric pressure discharges.

Dr. Tachibana is a member of The Japan Society of Applied Physics, the American Vacuum Society, and is serving as the President of the International Plasma Chemistry Society.